RESEARCH ARTICLE

Key Points:
- A rapid, high-resolution shipboard survey provided a unique 3-D view of an Arctic anti-cyclonic cold-core eddy on the Chukchi slope
- The winter water in the core contained high levels of nitrate, but the biological activity had largely ceased due to lack of sunlight
- The eddy was imbedded in the seaward edge of the Chukchi slope current and likely formed in the vicinity of Barrow Canyon

Correspondence to:
R. M. Scott,
ryacot85@bas.ac.uk

Three-Dimensional Structure of a Cold-Core Arctic Eddy Interacting with the Chukchi Slope Current

Ryan M. Scott[1,2] (iD), Robert S. Pickart[3] (iD), Peigen Lin[3] (iD), Andreas Münchow[4], Min Li[5], Dean A. Stockwell[6] (iD), and J. Alexander Brearley[1] (iD)

[1]British Antarctic Survey, Cambridge, UK, [2]Ocean and Earth Science, University of Southampton, Southampton, UK, [3]Department of Physical Oceanography, Woods Hole Oceanographic Institution, Woods Hole, MA, USA, [4]College of Earth, Ocean and Environment, University of Delaware, Newark, DE, USA, [5]Guangdong Province Key Laboratory for Coastal Ocean Variation and Disaster Prediction, Guangdong Ocean University, Zhanjiang, China, [6]College of Fisheries and Ocean Sciences, University of Alaska, Fairbanks, AK, USA

Abstract A rapid, high-resolution shipboard survey, using a combination of lowered and expendable hydrographic measurements and vessel-mounted acoustic Doppler current profiler data, provided a unique three-dimensional view of an Arctic anti-cyclonic cold-core eddy. The eddy was situated 50-km seaward of the Chukchi Sea shelfbreak over the 1,000 m isobath, embedded in the offshore side of the Chukchi slope current. The eddy core, centered near 150-m depth, consisted of newly ventilated Pacific winter water which was high in nitrate and dissolved oxygen. Its fluorescence signal was due to phaeopigments rather than chlorophyll, indicating that photosynthesis was no longer active, consistent with an eddy age on the order of months. Subtracting out the slope current signal demonstrated that the eddy velocity field was symmetrical with a peak azimuthal speed of order 10 cm s^{-1}. Its Rossby number was ~0.4, consistent with the fact that the measured cyclogeostrophic velocity was dominated by the geostrophic component. Different scenarios are discussed regarding how the eddy became embedded in the slope current, and what the associated ramifications are with respect to eddy spin-down and ventilation of the Canada Basin halocline.

Plain Language Summary A critical feature of the interior Arctic Ocean is the sharp vertical change in salinity between roughly 100-m to 200-m depth, known as the cold halocline. This shields the warm Atlantic-origin water below from mixing upward to the surface and melting the pack ice. The cold halocline is believed to be partially maintained by eddies of cold water emanating from the Chukchi Sea continental shelf. This paper presents measurements from a rapid, high-resolution shipboard survey of a cold-core Arctic eddy offshore of the shelf edge, providing a unique three-dimensional view of the feature. The eddy's core contained water near the freezing point with a high level of nitrate, but the biological activity had largely ceased because the eddy had descended below the part of the water column exposed to sunlight. The eddy was imbedded in the offshore edge of the westward-flowing Chukchi slope current. Different scenarios are discussed regarding how the eddy became embedded in the slope current, and what the associated ramifications are with respect to disintegration of the eddy and the manner in which the cold water feeds the halocline.

1. Introduction

The cold halocline is an important part of the water column of the Arctic Ocean, as its enhanced stratification prevents the warm Atlantic Water below from mixing vertically to the sea surface and melting the pack ice (Carmack et al., 2015). It is now well established that the cold halocline is ventilated laterally from the edges of the Arctic basin, rather than vertically from above (Aagaard et al., 1981). In the Canadian sector of the Arctic, dense winter water near the freezing point formed on the Bering, Chukchi, Beaufort, and East Siberian shelves provides source water for the cold halocline (Anderson et al., 2013; Melling, 1993; Muench et al., 1988; Weingartner et al., 1998). The cold water is also high in nutrients, in part because, during formation, regenerated nutrients from the sediments are mixed into the water column (Arrigo et al., 2017; Cooper et al., 1997). Hence the winter water contributes as well to the nutricline of the Canada Basin (Jones & Anderson, 1986), which impacts primary production. Above the cold halocline resides the summer Pacific halocline (e.g. Steele et al., 2004), whose constituent water masses originate from different
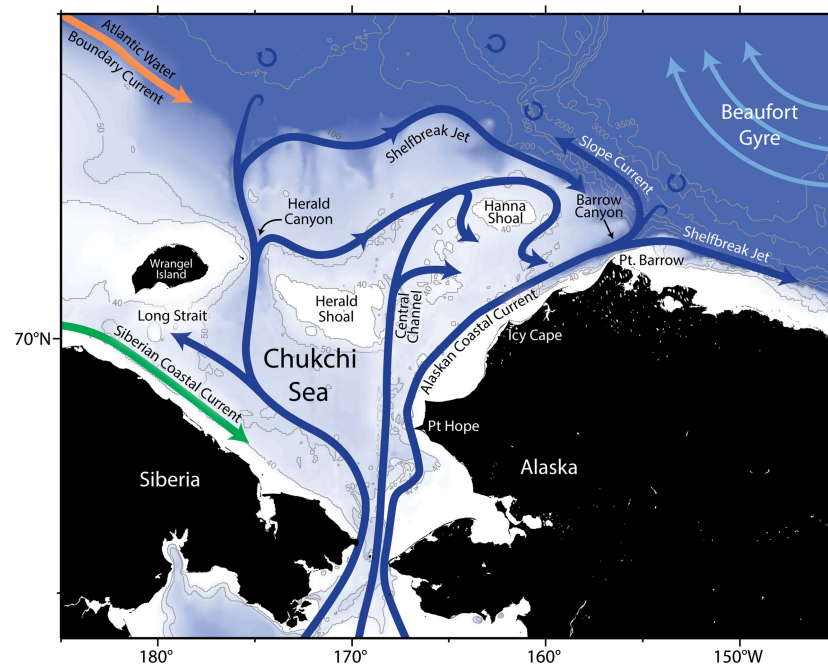
Figure 1. Schematic circulation of the Chukchi and Beaufort Seas, including place names (from Corlett & Pickart, 2017).

portions of the Bering Sea shelf during the warm months of the year. These warm waters are not considered in this paper, and from here-on the term halocline refers to the cold halocline, which has an upper portion and lower portion, separated by a salinity of roughly 33.5 (Pickart, 2004).

In order to ventilate the cold halocline, the dense winter water must be fluxed from the shelves into the interior basin. Figure 1 presents a circulation schematic for the vicinity of the Chukchi and Western Beaufort Seas. Pacific water is known to exit the Chukchi shelf through Barrow Canyon in the east (Pickart et al., 2005; Weingartner et al., 2017) and Herald Canyon in the west (Linders et al., 2017; Pickart et al., 2010). Both of these outflows form a shelfbreak jet that flows to the east. The Chukchi shelfbreak jet transports between 0.01 and 0.10 Sv of Pacific water (Corlett & Pickart, 2017; Li et al., 2019), while the transport of the Beaufort shelfbreak jet is in the range 0.02–0.13 Sv (Brugler et al., 2014; Nikolopoulos et al., 2009). Recently it has been documented that Pacific water is advected in a westward-flowing boundary current along the continental slope of the Chukchi Sea (Corlett & Pickart, 2017; Li et al., 2019). This current has been named the Chukchi slope current and is believed to emanate from Barrow Canyon (Spall et al., 2018). Corlett and Pickart (2017) constructed a mass budget of the Chukchi shelf, in which the slope current constitutes the dominant outflow. Transport estimates of the Pacific water component of the current range from 0.50 to 0.57 Sv (Corlett & Pickart, 2017; Li et al., 2019).

There are various mechanisms by which the Pacific water carried by the system of boundary currents stemming from the Chukchi shelf can be fluxed seaward into the basin. This can occur via wind-forced upwelling and downwelling at the shelfbreak. The former process has been studied extensively in the Beaufort Sea and occurs throughout the year during all ice conditions (e.g. Pickart et al., 2009, 2011, 2013; Lin et al., 2016). The offshore Ekman transport during these events carries Pacific water from the surface layer on the shelf into the basin (Ekman depth approximately 45 m, Schulze & Pickart, 2012). Although this water can be as cold as Pacific winter water during much of the year, it is typically too fresh (and light) to ventilate the halocline. Upwelling has also been observed on the Chukchi slope, although there is less evidence of an offshore surface Ekman circulation (Li et al., 2019). Downwelling, on the other hand, does transport Pacific winter water offshore in the density range of the upper halocline. This has been demonstrated in the Canadian Beaufort Sea (Dmitrenko et al., 2016) and in the Alaskan Beaufort Sea (Foukal et al., 2019).

Another mechanism for transporting Pacific winter water offshore is via eddies. Halocline eddies are a ubiquitous feature of the Canada Basin and are commonly observed by a variety of measurement platforms (e.g.

Manley & Hunkins, 1985; Plueddemann et al., 1999; Muench et al., 2000; Mathis et al., 2007; Kawaguchi et al., 2012; Zhao & Timmermans, 2015; Fine et al., 2018). The vast majority of the eddies are cold-core anti-cyclones with lateral scales on the order of the Rossby deformation radius, which is between 10 and 15 km in this region (Zhao et al., 2014). The eddies that reside in the northern part of the Canada Basin are generally shallow (centered above 80 m) and are believed to be spawned via baroclinic instability of the hydrographic front that divides Canadian Arctic waters from Eurasian Arctic waters (Timmermans et al., 2008). By contrast, the cold-core anti-cyclones observed in the southern portion of the Canada Basin are deeper (centered below 80 m), saltier, and denser. These features are believed to last up to a year before spinning down, and their population has increased in recent years (Zhao et al., 2016).

The deeper cold-core eddies found in the southern Canada Basin are thought to emanate from the two canyons on the outer Chukchi shelf or from the boundary currents that emerge from these canyons. Numerical, laboratory, theoretical, and observational studies have argued that the dense water flowing down Barrow Canyon should form anti-cyclonic eddies, either through sidewall friction (D'Asaro, 1988), flow-topography interactions (Cenedese & Whitehead, 2000; Chao & Shaw, 2003), or baroclinic instability (Pickart et al., 2005). Pickart and Stossmeister (2008) present MODIS satellite ice images showing a train of anti-cyclones being generated from the canyon outflow, which provides observational support for these mechanisms. Presumably the same argument applies to the Herald Canyon outflow. Indeed, Pisareva et al. (2015) observed a cold-core anticyclone of Pacific winter water situated directly offshore of the mouth of the canyon.

It is also believed that Pacific winter water anti-cyclones are spawned from the shelfbreak jet of the Chukchi and Beaufort Seas via baroclinic instability. This process was investigated by Spall et al. (2008) who used mooring observations to assess the stability characteristics of the Beaufort shelfbreak jet and to calculate the mean-to-eddy energy fluxes. This implied that baroclinic instability was active, and the numerical model they employed showed how the unstable boundary current readily formed eddies with the same characteristics of those observed in the basin. The Chukchi shelfbreak jet should be similarly unstable, and Pickart et al. (2005) presented evidence of a cold-core anti-cyclone being spawned from the current. It remains to be determined if the Chukchi slope current can form Pacific water eddies. Corlett and Pickart (2017) showed that the potential vorticity structure of the current satisfies the necessary condition for baroclinic instability, and the current undergoes meanders which are suggestive of an unstable current. The eddies spawned from the canyon outflows and boundary currents are represented schematically in Figure 1. Pickart et al. (2005) argued that, in order for the locus of these eddies to be the dominant ventilation source of the Canada Basin upper halocline, 100–200 eddies must be formed each year. This does not seem unreasonable in light of the large numbers of cold-core anti-cyclones observed in the basin (e.g. Zhao et al., 2014).

While anti-cyclonic cold-core eddies have been observed extensively in the Canada Basin, most notably using the ice-tethered profiler database, to date there have been no surveys revealing the full three-dimensional structure of one of these features. In addition, no studies have investigated the role of the Chukchi slope current in either generating or influencing the eddies. In this paper we present results from a high-resolution shipboard survey of a cold-core anti-cyclonic Pacific water eddy. The feature was situated on the Chukchi continental slope to the northwest of Barrow Canyon, adjacent to the seaward edge of the Chukchi slope current. The eddy, and its immediate surroundings, was mapped using a combination of expendable probes, lowered instrumentation, and underway sensors. The uniform horizontal grid spacing in both longitude and latitude provided an unprecedented three-dimensional view of the feature. We begin with a description of the data, followed by an analysis of the eddy's water mass, kinematic, and dynamical structure. The Chukchi slope current is then investigated in an effort to better understand the interaction between the current and the eddy. Finally, we discuss some of the implications of our findings.

2. Data and Methods

2.1. Hydrographic Data

The in situ data used in this study were collected in September 2004, on the USCGC *Healy*, as part of the Western Arctic Shelf Basin Interactions program. The ship sampled both the Chukchi and Alaskan Beaufort Seas, but the geographical focus of the present study is the Chukchi continental slope to the south of the Northwind Ridge (Figure 2). Different aspects of this eddy have been reported on earlier, addressing the off-shelf flux of carbon (Mathis et al., 2007), the age of the eddy determined by radium dating (Kadko
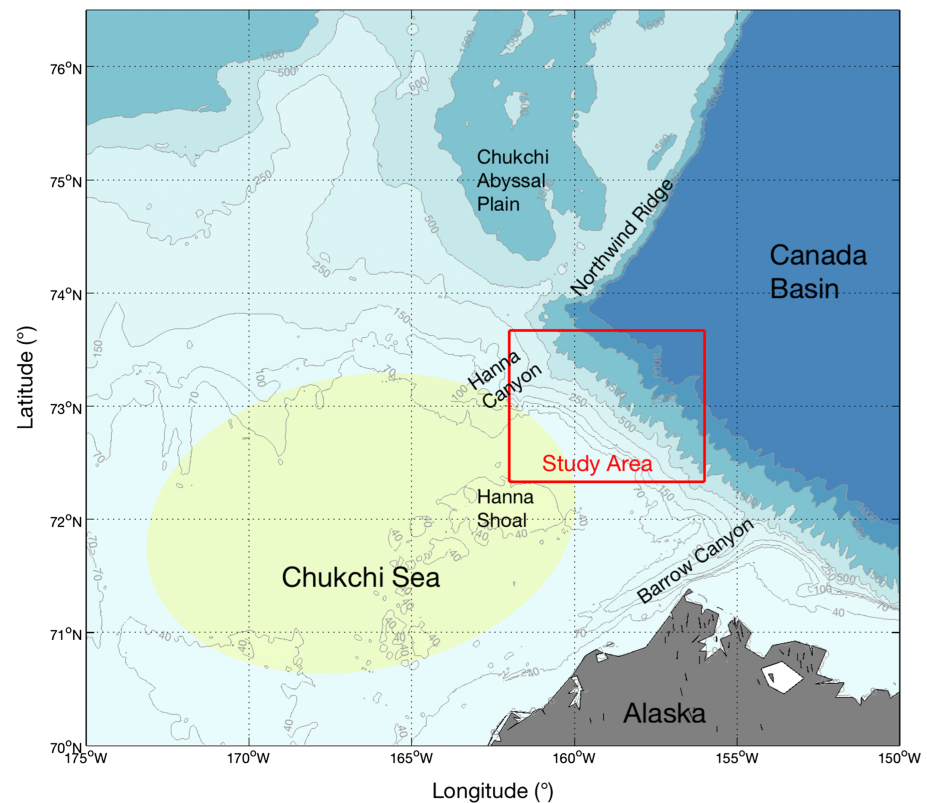
Figure 2. Study domain and place names. The bathymetry is from IBCAO v3 (Jakobsson et al., 2012). The area outlined in red is shown in Figure 3. The yellow shaded area on the Chukchi shelf is where the wind stress curl was averaged to construct the time series of Figure. 15.

et al., 2008), and the different zooplankton species contained within the feature (Llinás et al., 2009). Here we focus mainly on the physical attributes of the eddy.

The eddy was initially revealed by occupying a series of expendable-bathythermograph (XBT) sections across the Chukchi continental slope (sections x1–x5; Figure 3a). Only the western-most line (x1, which was occupied first) showed any evidence of an eddy. After completing section x5, we steamed back to section x2 and did a back-and-forth XBT line (x6), in order to pinpoint the location of the eddy core and determine its along slope length scale. Using this information, we laid out a high-resolution grid to be occupied as quickly as possible using expendable conductivity-temperature-depth (XCTD) probes (Figure 3b). Due to inventory constraints, *Healy's* CTD package was used to complete Transect 1 and extend XCTD Transect 2 (green squares). The CTD casts were taken to 300 m, and no water sampling was done in order to save time.

The average station spacing of the eddy grid was 5 km, and it took approximately 24 hr to complete. This resulted in a synoptic snapshot encompassing the eddy with uniform spatial coverage. This is the only such survey resolving the complete three-dimensional structure of an Arctic eddy of which we are aware. Approximately 4 hr after the XCTD survey was completed, a CTD section was occupied across the center of the eddy. This took 25 hr to complete and included water sampling for dissolved oxygen, total CO_2, nutrients, total alkalinity, chlorophyll, dissolved and particulate organic matter, and salinity. At six of the stations a multi-net cast was done to sample for zooplankton. Many of the biochemical aspects of the eddy are reported elsewhere (Mathis et al., 2007; Kadko et al., 2008; Llinás et al., 2009).

The CTD used on the *Healy* was a Sea-Bird 911+ with dual temperature and conductivity sensors mounted on a 24-place rosette with 12-L Niskin bottles. Laboratory calibrations were done on the temperature sensors, and the conductivity data were calibrated using the bottle salinity data. The accuracies were deemed to be 0.001 °C and 0.007 for temperature and salinity, respectively. Additional CTD variables included transmissivity and fluorescence, although these were not calibrated. The final CTD data were used to create 1-db
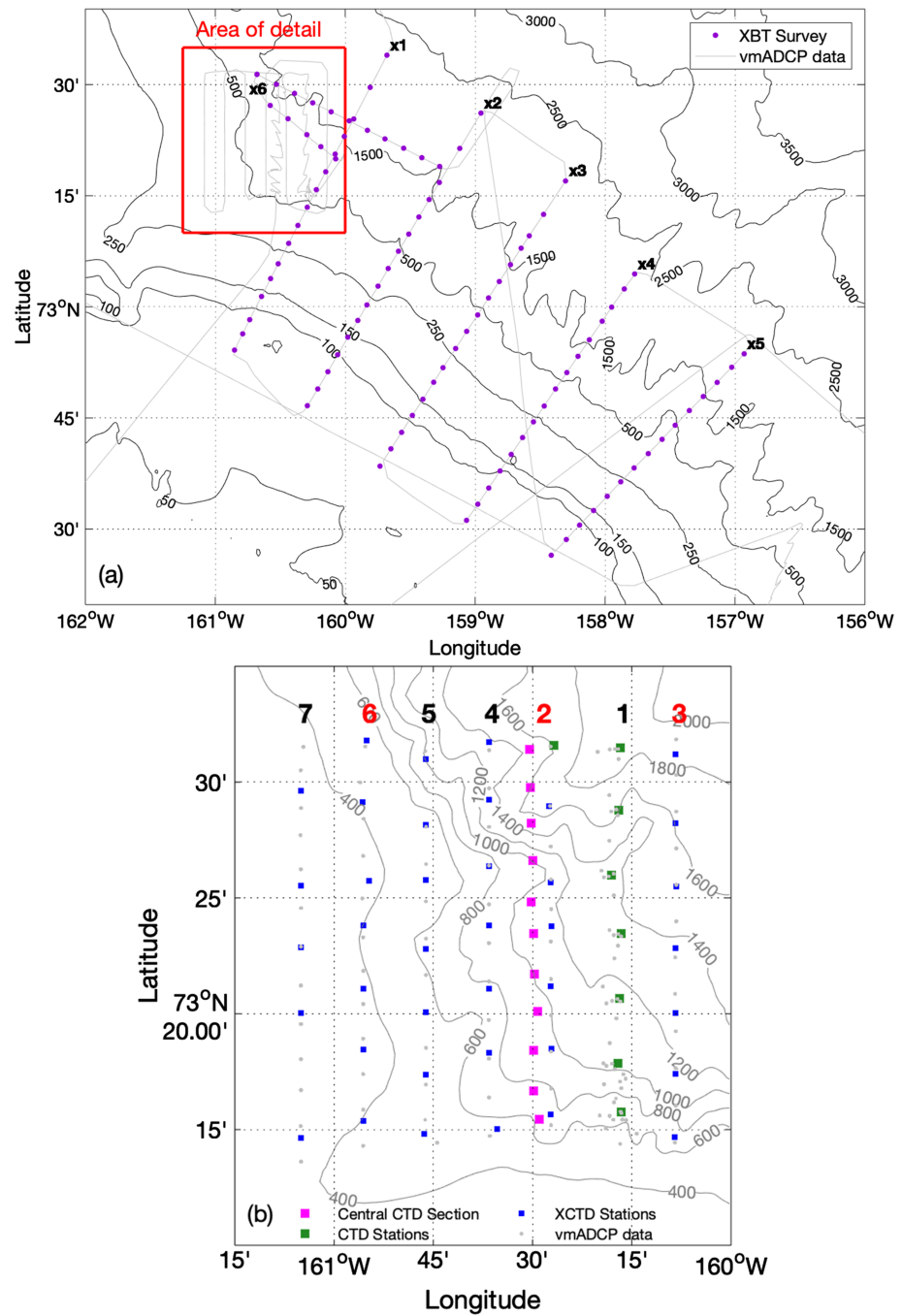
Figure 3. (a) Expendable-bathythermograph (XBT) transects occupied in order to locate the eddy (the XBT drops are denoted by the purple dots). The ship track is indicated by the gray lines. The area of detail outlined in red is shown in (b). The black lines are the bathymetry contours from IBCAO v3 (Jakobsson et al., 2012). (b) The eddy survey consisting of expendable conductivity-temperature-depth (XCTD) stations (blue squares), CTD stations (magenta and green squares), and vessel-mounted acoustic Doppler current profiler (ADCP) profiles (grey dots). The transect numbers of the grid are indicated along the top (the central CTD section [magenta square] is not considered part of the synoptic grid). The three transects highlighted in red are shown in Figures 4 and 10. The bathymetry is from the ship's multi-beam system.

averaged downcast files. Kadko et al. (2008) describe the processing and calibration of the XCTD data. The XCTD temperature, salinity, and depth are deemed accurate to within 0.02 °C, 0.04, and 1 m, respectively. The final XCTD data were used to construct 2-m averaged profiles of temperature and salinity. Both the

CTD and XCTD data were used to calibrate *Healy's* multi-beam system, which produced the bathymetry used in the "area of detail" figures (Figures 3b, 6, 9, and 11).

Vertical sections of various properties were constructed using Laplacian-Spline interpolation with a vertical grid spacing of 5 m and horizontal grid spacing of 1 km, where the meridional distance is relative to the latitude of 73.24°N (which is just south of the XCTD survey minimum latitude). Lateral plots were constructed using the same interpolator, with a grid spacing of 0.01° in latitude and 0.02° in longitude. The lateral maps do not include the hydrographic or velocity data from central CTD section because, as noted above, it took approximately 25 hr to occupy the section after the eddy survey was completed.

2.2. Velocity Data

Vessel-mounted acoustic Doppler current profiler (VMADCP) data were obtained from *Healy's* 75-kHz phased-array Ocean Surveyor instrument. Attitude information (heading, pitch, and roll) was provided by an Ashtech ADU2-3DGPS receiver, and the ship's position was determined by a Trimble Centurion p-code DGPS system. Processing and merging of these data streams resulted in calibrated, earth-referenced profiles of horizontal currents from about 20 m below the surface to a maximum depth of 400-m depth every 2 min in 15-m vertical bins. The reader is referred to Münchow et al. (2006, 2015) for details about the system and its overall performance. As part of the quality control of the velocity data set, we sorted the data within each 2-min interval and discarded extreme values from the record. We thus forced the data distribution towards a normal distribution for which the standard deviation decreases as $N^{-1/2}$, where N is the number of independent estimates (pings). With a single ping error of about 14 cm s^{-1} and $N = 50$ pings within each 2-min ensemble, we estimate absolute random errors to be about 2 cm s^{-1}. For the analysis we created 10-min averages of the ensembles.

Based on mooring data from Chukchi continental slope, tidal velocities in this region are small (<2.2 cm s^{-1}; Li et al., 2019). Nonetheless, the major barotropic tidal signals were removed from the VMADCP profiles using the Oregon State University Arctic tidal model, which has a resolution of 5 km and predicted similarly small tides (<2 cm s^{-1}; Padman & Erofeeva, 2004; Llinás et al., 2009). Sections of relative geostrophic velocity were calculated from the dynamic height relative to the sea surface using the gridded CTD data. These velocities were subsequently interpolated to the original grid, then made absolute by referencing them to the analogously gridded VMADCP velocities. In particular, for each grid point, the vertically averaged relative geostrophic velocity was matched to the vertically averaged cross-track VMADCP velocity over their common depth range. This resulted in vertical sections of absolute geostrophic velocity along each transect.

2.3. Biochemical Data

Chlorophyll a and phaeopigments were determined fluorometrically (Holm-Hansen et al., 1965) by filtration through 25-mm Whatman GF/F filters as outlined in Evans et al. (1987). Samples were collected from the CTD casts and immediately filtered. The filters were placed in vials on ice, sonicated in 90% acetone, and extracted for 24 hr. Extracted fluorescence was measured before and after acidification (10% HCL), with a Turner Designs model AU-10 fluorometer calibrated with commercially purified Chlorophyll a (Turner Designs).

Sample methods for nutrients have already been described in detail elsewhere (see Codispoti et al., 2005). In brief, nutrient analyses (phosphate, silicate, nitrate + nitrite, urea, ammonium, and nitrite) were performed on an ODF-modified 6-channel Technicon AutoAnalyzer II. The samples collected from CTD casts were generally analyzed within a few hours after sample collection. Methodologies and modification for the individual nutrient species are also described in detail in Codispoti et al. (2005).

2.4. Wind and Surface Geostrophic Velocity Data

Timeseries of wind stress curl over the Chukchi shelf were constructed using 10-m wind fields from the ERA-Interim reanalysis provided by the European Center for Medium-Range Weather Forecasts (Berrisford et al., 2009). The data have a temporal and spatial resolution of 6 hr and 0.75°, respectively. The surface geostrophic velocity during the time period of the eddy survey was provided by Copernicus Marine and Environment Monitoring Service (http://marine.copernicus.eu/). This product consists of daily gridded fields with a resolution of 0.25° in latitude and longitude, based on data from multiple altimeter missions.
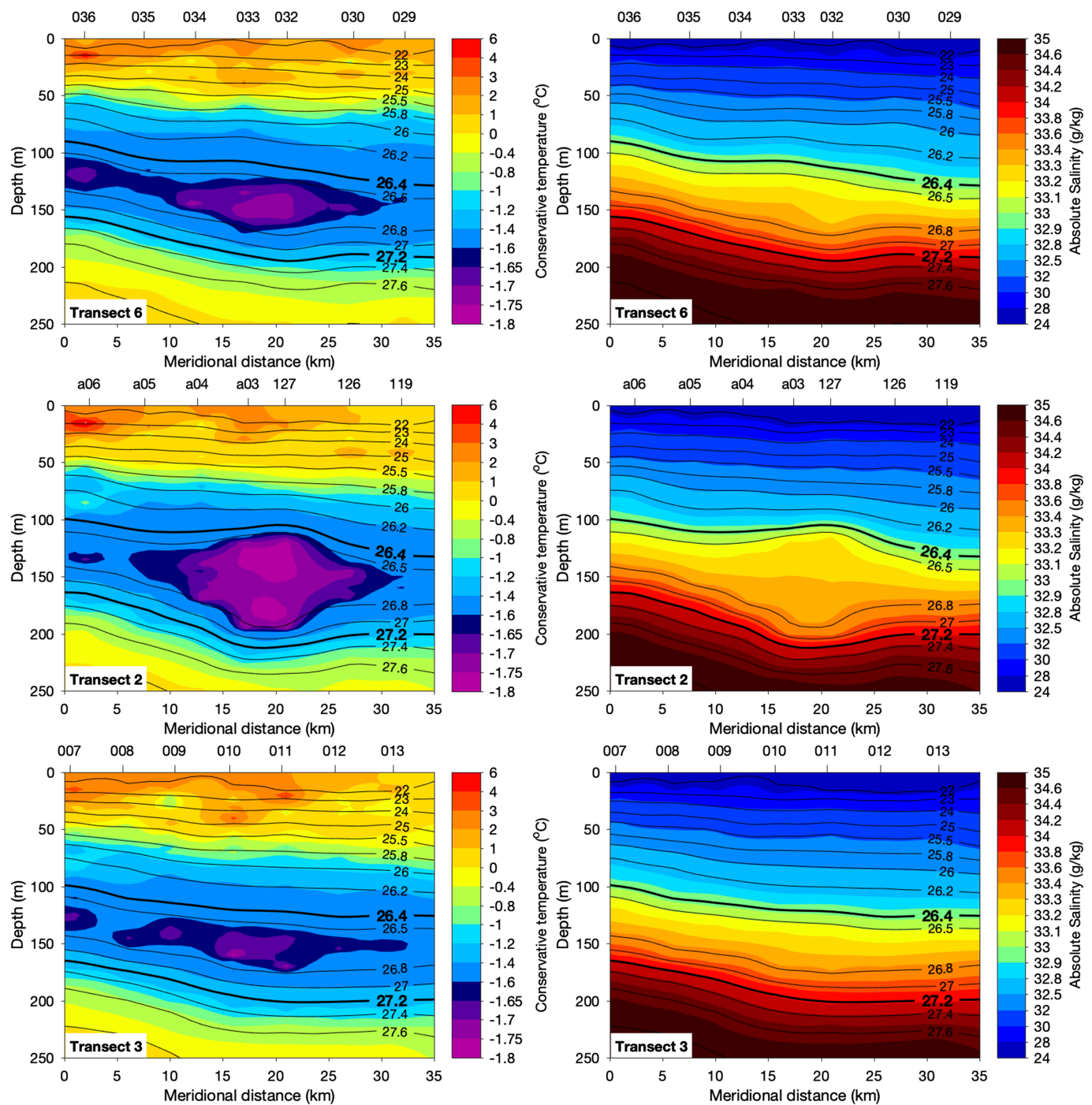
Figure 4. Vertical expendable conductivity-temperature-depth sections of (left panel) conservative temperature and (right panel) absolute salinity through the eddy, overlain by potential density (contours, kg m^{-3}). See Figure 3b for the locations of the three transects. The viewer is looking to the west. Station numbers are marked along the top (Station 119 is a conductivity-temperature-depth cast). The highlighted density contours correspond to the layer averages in Figures 9 and 11.

3. Results

3.1. Eddy Hydrographic Characteristics

Cross-slope vertical sections from the XCTD grid reveal that the feature was a cold-core eddy centered vertically near 150-m depth (Figure 4), embedded within the halocline, roughly confined to the density layer 26.4–27.2 kg m^{-3}. On the western side (Transect 6, Figure 4 top row) there is only a slight widening of
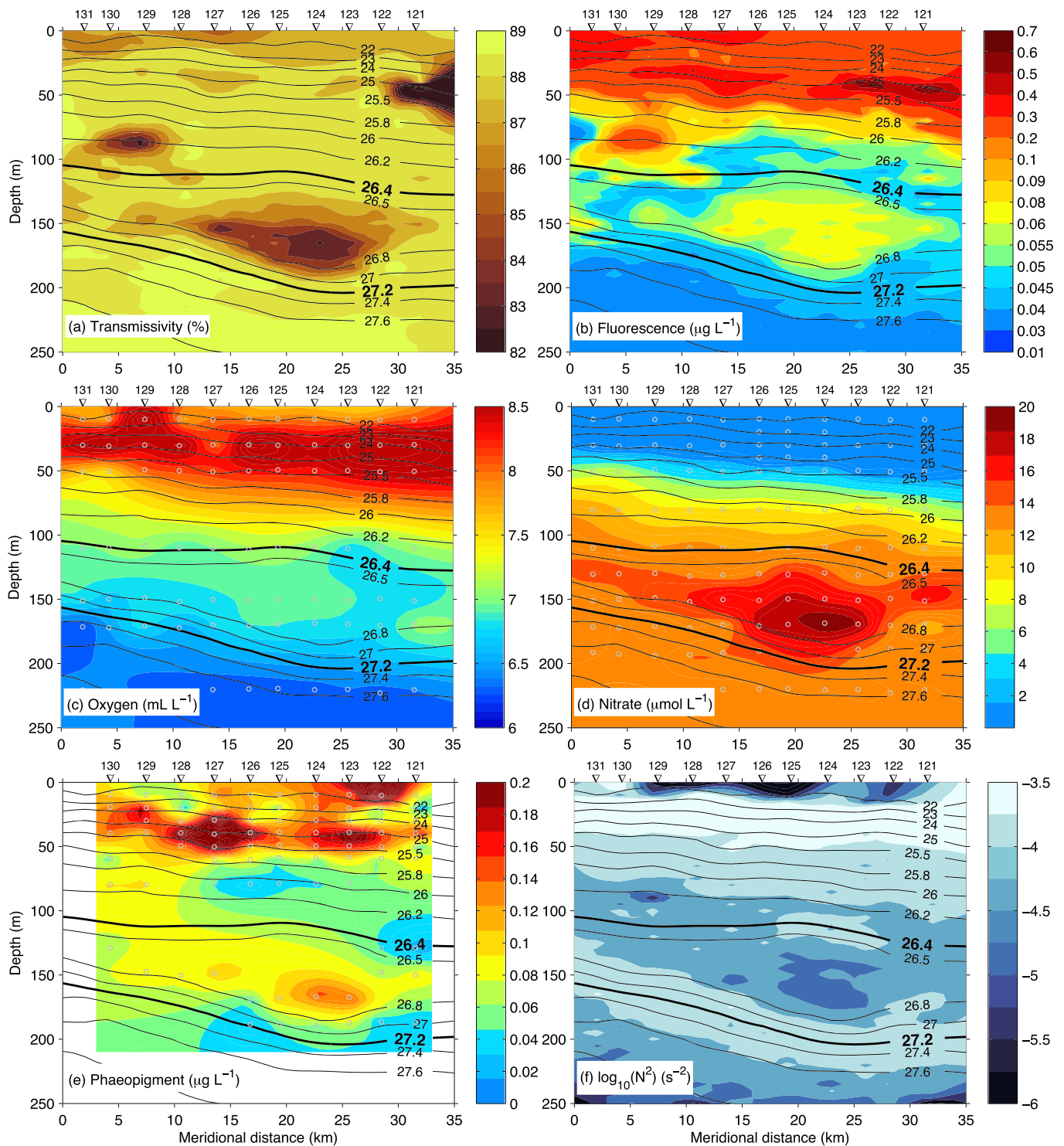
Figure 5. Vertical sections through the center of the eddy using data from the conductivity-temperature-depth and Niskin bottles (see Figure 3b, magenta squares, for the location of the section). The viewer is looking to the west. Station numbers are marked along the top. In each panel the contours are potential density (kg m^{-3}). The highlighted density contours correspond to the layer averages in Figures 9 and 11.(a) transmissivity; (b) fluorescence; (c) oxygen, where the bottle data points are indicated by the open grey circles; (d) nitrate; (e) Phaeopigments; and (f) log of the buoyancy frequency squared.

this density layer corresponding to a lens of cold water less than −1.6 °C, approximately 45-m thick, and centered laterally near a meridional distance of 20 km. Near the eddy center (Transect 2, Figure 4 middle row) the temperature is colder, with a core value of −1.77 °C, and the layer thickness doubles to ~9 m. On
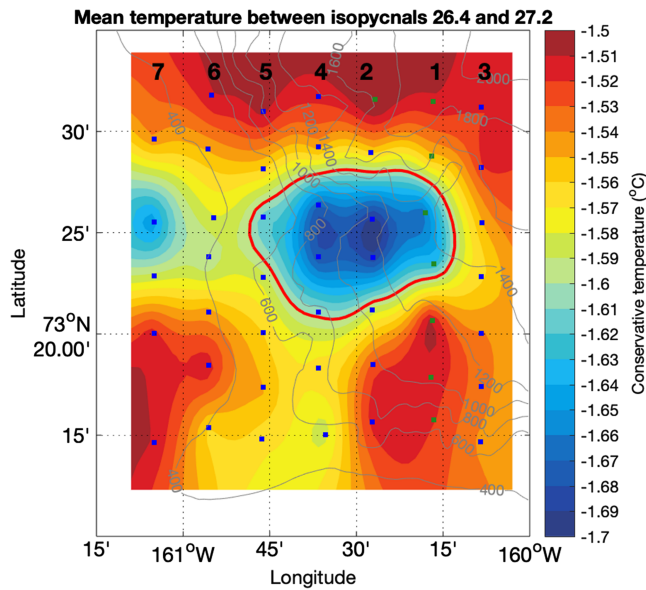
Figure 6. Conservative temperature averaged within the density layer 26.4–27.2 kg m^{-3} (see Figure 4 for the location of the layer in the vertical plane). The −1.6 °C contour, taken to delimit the core of the eddy, is highlighted red. The expendable conductivity-temperature-depth stations are marked by the blue squares, and the conductivity-temperature-depth stations are marked by the green squares. The transect numbers are labeled along the top. The bathymetry is from the ship's multi-beam system.
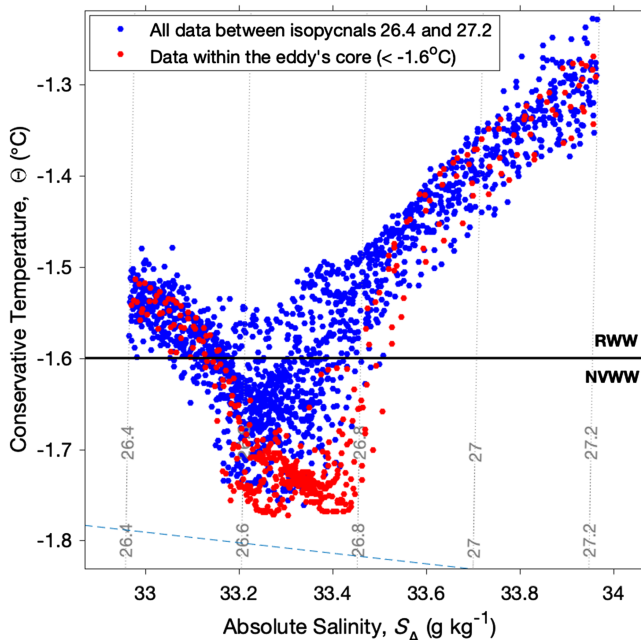

Figure 7. /S_A scatter plot for the expendable conductivity-temperature-depth/conductivity-temperature-depth data points within the density layer 26.4–27.2 kg m^{-3} (see Figure 4 for the location of the layer in the vertical plane). Data are taken from all stations shown in Figure 6. The data points within the core of the eddy are highlighted red (see Figure 6 for where the core of the eddy is situated). The thin grey lines are contours of potential density (kg m^{-3}). The thick black line shows the division between the newly ventilated winter water (NVWW) and remnant winter water (RWW); see text for details. The freezing point is marked by the dashed blue line.

the eastern side of the feature (Transect 3, Figure 4 bottom row) the cold layer is only ~30-m thick, and there is little to no widening of the density layer. At these cold temperatures the density is dictated by salinity, and only the transect through the eddy center shows a noticeable signature of the isohalines, which spread apart from the core absolute salinity of 33.3 g kg^{-1}. This core value corresponds to the upper halocline in the southern Canada Basin (Melling, 1998; Pickart, 2004).

The cold water within the eddy corresponds to newly ventilated winter water (NVWW), which is formed via convection in the Bering Sea (e.g. Muench et al., 1988) and Chukchi Sea (e.g. Pickart et al., 2016), and is colder than −1.6 °C and saltier than 31.5 (e.g. Pisareva et al., 2015; Corlett & Pickart, 2017). The other type of winter water is known as remnant winter water (RWW), which is NVWW that has warmed either by mixing or via solar heating (Gong & Pickart, 2016). It should be noted that most of the NVWW is typically flushed off of the Chukchi shelf by late summer (Pickart et al., 2019; Shroyer & Pickart, 2019).

The CTD section through the center of the cold-core eddy (Figure 3b, magenta squares) provides additional information about the feature (Figure 5). Transmissivity within the eddy is lower than the surrounding water (Figure 5a). Some of this is likely due to suspended sediments since the dense NVWW flows along the bottom of the Chukchi shelf as it progresses northward (prior to eddy formation near the shelf edge). However, the elevated values of fluorescence (Figure 5b) and dissolved oxygen (Figure 5c) indicate recent biological activity. It is well documented that primary production on the Chukchi shelf is strongly tied to the presence of winter water (e.g. Lowry et al., 2015, 2018). This is because winter waters are generally high in nutrients. In fact, the NVWW has the highest levels of nitrate on the Chukchi shelf during early summer (Pickart et al., 2016). The eddy also contained elevated levels of nitrate sufficient to spur primary production (Figure 5d). However, the depth of the core was well beneath the euphotic zone (typically <25 m at this time of year), implying that photosynthesis completely ceased once the eddy left the edge of the shelf and descended to its equilibrium depth.

The lack of photosynthesis is consistent with the low levels of chlorophyll within the eddy (not shown), while there was an enhanced phaeopigment signal (Figure 5e). This implies that the chlorophyll cells in the feature were either dead and or in the process of dying, which is expected when nutrients are drawdown, or, in this case, the access to sunlight is cut off. It should be noted, however, that phaeopigments do fluoresce, which accounts for the signal in Figure 5b. Using radium isotope data, Kadko et al. (2008) estimated the age of the eddy to be on the order of months (i.e. the time since it left the shelf). The chlorophyll to phaeopigment differential that we measured is consistent with this time frame (i.e. significantly shorter than a year). In addition, the weak stratification of the eddy core (Figure 5f), and the fact that it contains NVWW, suggests that the water in the feature was ventilated earlier in the year during the winter months, as opposed to the previous winter. This is because NVWW is modified fairly quickly into RWW (Gong & Pickart, 2016). This supports the radium age estimate as well.

A lateral map of the mean temperature within the density layer bounding the eddy (26.4–27.2 kg m^{-3}, shown in the vertical sections
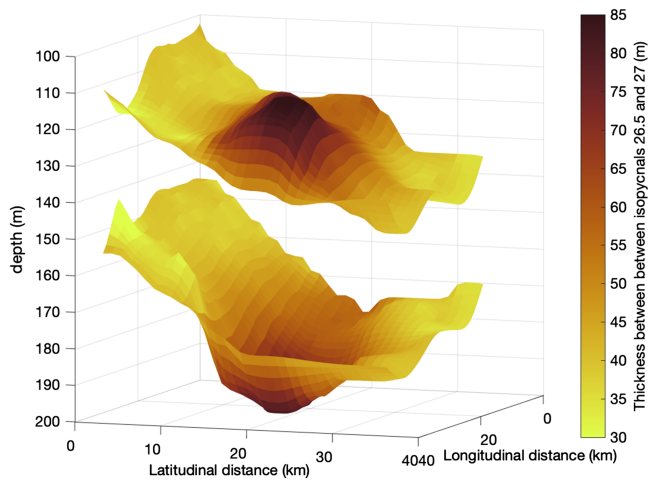
Figure 8. Three-dimensional view of two isopycnal surfaces, 26.5 and 27 kg m^{-3}, near the top and bottom of the eddy, respectively. The color corresponds to the thickness of the layer bounded by the two isopycnals.

of Figures 4 and 5) indicates that the XCTD survey completely encompassed the feature (Figure 6). The eddy's core, defined here as within the −1.6 ° C isotherm, has a quasi-circular shape, with a zonal diameter of ~19 km and a meridional diameter of ~14 km. It is located over the deep continental slope, centered on the 1,000-m isobath, roughly 50-km seaward of the shelfbreak. The water surrounding the eddy displays some patchiness in temperature, particularly to the west and south, which could be a reflection of mixing processes as the eddy spins down (see the Discussion section).

A conservative temperature–absolute salinity (/S$_A$) diagram characterizes the water in the survey region between the bounding isopycnals of the eddy (Figure 7). As noted above, the water in the core of the eddy is NVWW. The coldest water in the eddy is predominantly confined to the density layer 26.6–26.8 kg m^{-3}, and, at the center of the feature, the temperature is near the freezing point (−1.8 °C at this temperature and salinity). Even outside of the eddy some of the water is NVWW, although most of the surrounding water is slightly warmer RWW, which is the dominant water mass of the cold halocline in the Canada Basin. As the eddy spins down, the anomalously cold NVWW in its core will moderate to RWW.

The rapid, high-resolution XCTD grid allows us to present the first three-dimensional view of an Arctic cold-core anti-cyclone. In Figure 8 we show the topography of the bounding density layers 26.5 and 27 kg m^{-3} (these surfaces are slightly more restrictive than those used above in order to highlight the deflection of the isopycnals), where the viewer is looking to the southwest. The maximum layer thickness is 85 m, compared to a thickness of 37 m outside of the eddy. Note that the entire feature is slanted in the vertical; that is, the density surfaces are shallower on the onshore side of the eddy versus the offshore side. This background density tilt is also evident in the vertical sections of Figure 4. It is due to the presence of the Chukchi slope current, as explained below.
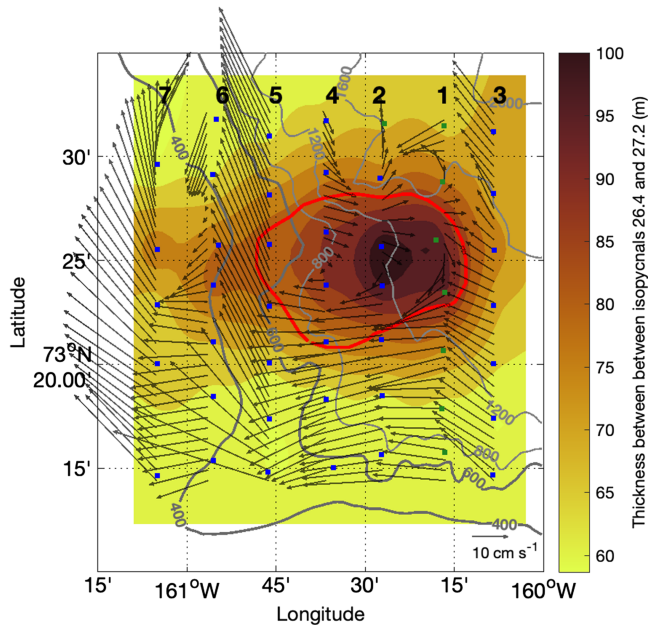
3.2. Eddy Kinematics and Dynamics

The vertical coverage of the VMADCP data extended on average to approximately 225-m depth, which enabled us to capture the three-dimensional velocity structure of the eddy and the surrounding flow (see Figures 3a and 3b for the lateral coverage of the VMADCP data). Figure 9 shows the vertically averaged velocity within the density range 26.4–27.2 kg m^{-3} (the same density layer as in Figure 6) in relation to the thickness of the layer. The azimuthal anti-cyclonic flow of the eddy is evident. However, it appears that the circulation of the feature is asymmetric, with enhanced flow on the southern side of the eddy versus the northern side. In addition, there is strong flow in both the western (sections 5–7) and eastern (section 3) parts of the domain. These aspects of the circulation are due to the fact that the eddy is embedded in the off-shore part of the Chukchi slope current.

Figure 9. Vessel-mounted acoustic Doppler current profiler velocity averaged within the density layer 26.4–27.2 kg m^{-3} (black vectors; the key is located in the lower right). The color represents the thickness of the density layer, and the red line denotes the core of the eddy (see Figure 6). The expendable conductivity-temperature-depth stations are marked by the blue squares, and the conductivity-temperature-depth stations are marked by the green squares. The transect numbers are labeled along the top. The bathymetry is from the ship's multi-beam system. The 400 and 600 m bathymetry contours are thicker, highlighting the sharp bend in bathymetry.

To demonstrate this more clearly, in Figure 10 we present vertical sections of absolute geostrophic velocity corresponding to the same three transects shown in Figure 4. The azimuthal flow of the eddy is clearly evident in Transect 2 through the center of the feature (compare to the temperature section through the center of the feature, Figure 4, middle row). However, in all three transects of Figure 10 the strongest westward flow is in the southern portion of the section above 50 m, which is the signature of the Chukchi slope current. At this time of year the slope current is
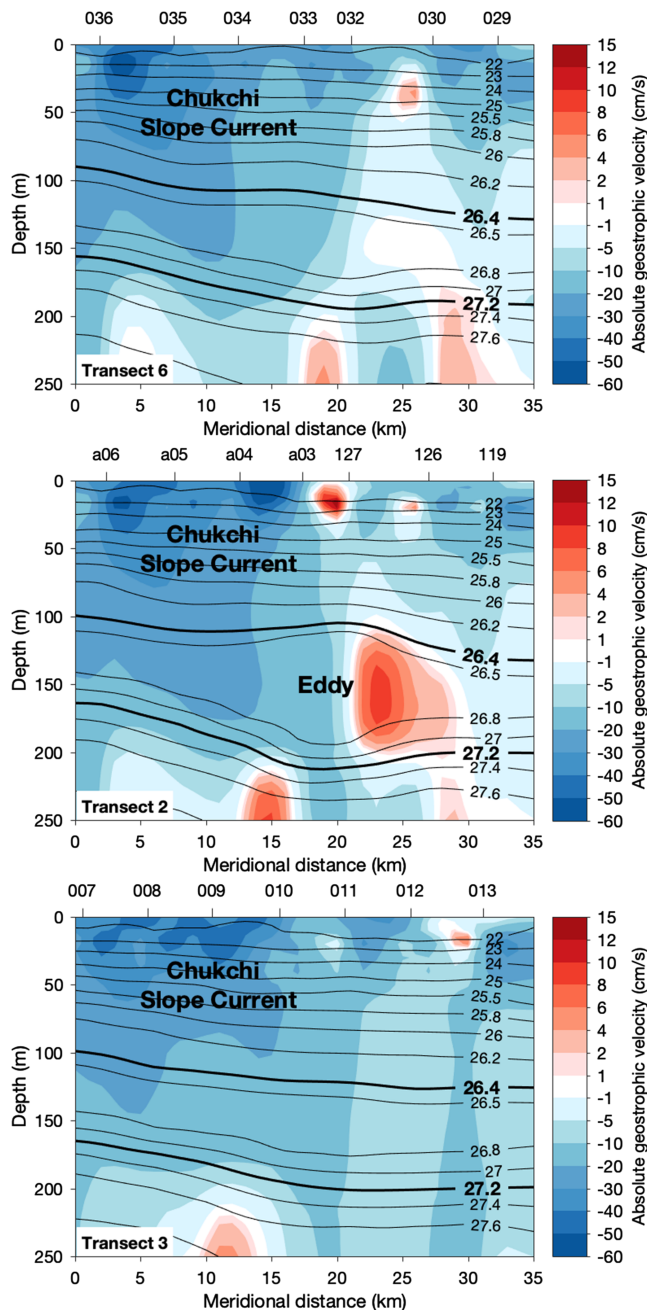
Figure 10. Vertical sections of absolute geostrophic velocity (color) overlain by potential density (contours, kg m^{-3}). See Figure 3b for the locations of the three transects. The viewer is looking to the west. Positive flow is to the east. Station numbers are marked along the top (Station 119 is a conductivity-temperature-depth cast). The highlighted density contours correspond to the layer averages in Figures 9 and 11. The Chukchi Slope Current is labeled as is the center of the eddy.

surface-intensified and extends to 150–200-m depth (Corlett & Pickart, 2017; Li et al., 2019). Based on data from a year-long mooring array across the Chukchi Slope, the mean transport of the current in early fall is 1.0 ± 0.48 Sv. This compares well to our September survey data; the transport of the slope current in Transects 6 and 3 (away from the eddy core) were both 0.83 Sv, where transports were calculated over the domain 0–21 km in distance and 0–185 m in depth.

As discussed above, the vertical sections of hydrographic properties for Transects 6 and 3, through the western and eastern sides of the eddy, respectively, show relatively little signature in the density field but a clear signal of cold NVWW (Figure 4). The absolute geostrophic velocity sections on the two sides of the eddy show a much more muted signal than the central transect (Figure 10). On the western side (Figure 10, Transect 6) there is just a hint of positive flow on the northern side of the eddy, while on the southern side there is no extremum of negative flow; the flow of the slope current masks any signature of this half of the eddy. On the eastern side (Figure 10, Transect 3), one would not notice that there is an eddy signature at all. These sections clearly demonstrate that the eddy is caught in the seaward side of the Chukchi slope current. Figure 9 indicates that the strong westward flow of the slope current in the southern portion of the domain (Transects 1–4) bends to the northwest on the western side of the domain (Transects 5–7). This deflection of the slope current is likely in response to the northward diversion of the isobaths due to Hanna Canyon (see Figures 2 and 3a).

In order to isolate the velocity signature of the eddy, we attempted to remove the signature of the slope current from the VMADCP data. The layer-averaged velocity vectors on Transect 4 (Figure 9) display the signature of a Rankine vortex for the northern half of the feature. This structure of intrahalocline Arctic eddies has been noted previously (Zhao et al., 2014). In particular, the eastward velocity increases from the eddy center until a maximum at the edge of the eddy (indicated by the red line in Figure 9). We assume therefore that the northern half of the eddy for Transect 4 is not significantly influenced by the slope current. We thus mirror the eddy signature about its center and subtract it from the full velocity section. This leaves values of 0 cm s^{-1} north of the eddy's center and an undisturbed signature of the slope current in the southern half of the section. Following this, we subtract the undisturbed slope current signal from the southern halves of Transects 1,2, and 4, which encompass the strongest part of the eddy. (We are unable to objectively remove the slope current signature in Transect 3 and after the current bends to the northwest in Transects 5–7.)

A more symmetrical eddy signature with peak azimuthal speeds of 8 cm s^{-1} appears in the layer-averaged velocity plot once it is isolated as described above (Figure 11; by definition it has to be symmetrical at Transect 4). A three-dimensional view, displaying both the eddy velocity field and the temperature field, is shown in Figure 12. At the topmost surface (100 m) there is little indication of the eddy: no NVWW is present, and there is no consistent swirl signature. As one progresses downward through the feature (125, 150, 175 m) the cold core becomes evident, as does the anti-cyclonic azimuthal flow. At the bottom of the feature (200 m) the swirl speed remains strong. This is consistent with the modeling results of Spall et al. (2008) that show that the velocity signal of cold-core Arctic eddies often extends deeper into the water column than the property signature.
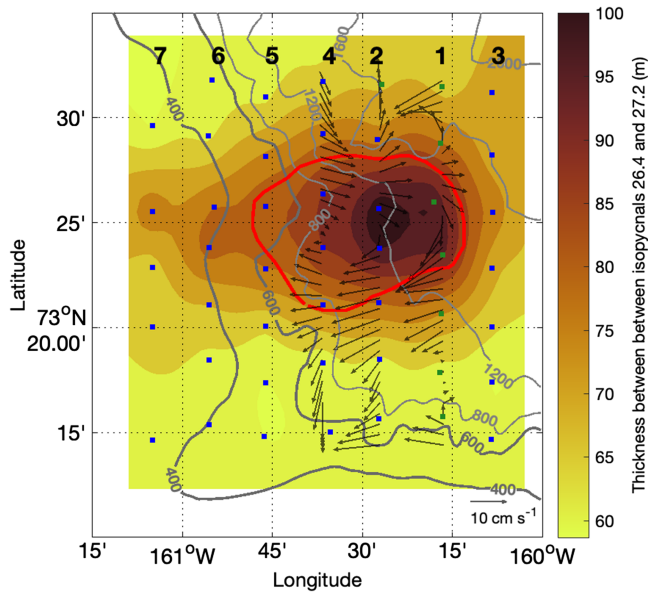
Figure 11. Same as Figure 9 except that the slope current signature has been removed (see text for details).

Previous studies have demonstrated that intrahalocline eddies are in cyclostrophic balance for large Rossby numbers (near 1) and in approximate geostrophic balance for small Rossby numbers (Fine et al., 2018; Zhao et al., 2014). To assess the dynamical balance in the eddy sampled here, we evaluated the cyclogeostrophic equation

$$\frac{v^2}{r} - fv - \frac{1}{\rho}\frac{\partial p}{\partial r} = 0, \tag{1}$$

where v is the eddy azimuthal velocity, r is distance from the eddy core, and f is the Coriolis parameter (1.3×10^{-4} s^{-1}). In equation (1) the first term on the left is the centrifugal acceleration, the second term is the Coriolis acceleration, and the third term is the pressure gradient force. We computed the three terms for Transect 2 (the XCTD line that passes through the eddy's center), averaged between the isopycnals 26.4–27.2 kg m^{-3} (the same density layer as in Figure 6). We find that the cyclogeostrophic velocity, the full solution to equation (1), is dominated by the geostrophic component (the balance of the two right-hand terms in equation (1); Figure 13a, where both velocity terms are referenced to 250 m). This is not surprising in light of the relatively weak swirl speeds of the feature (Figure 11). The Rossby number can be calculated as $R_o = \zeta/f$, where in cylindrical coordinates the relative vorticity $\zeta = \frac{\partial(rv)}{r\partial r}$.

Figure 13b shows how R_o varies across Transect 2. The maximum value on the two sides of the feature is ~0.4, suggesting a geostrophic balance. This is consistent with the warm-core eddy sampled by Fine et al.
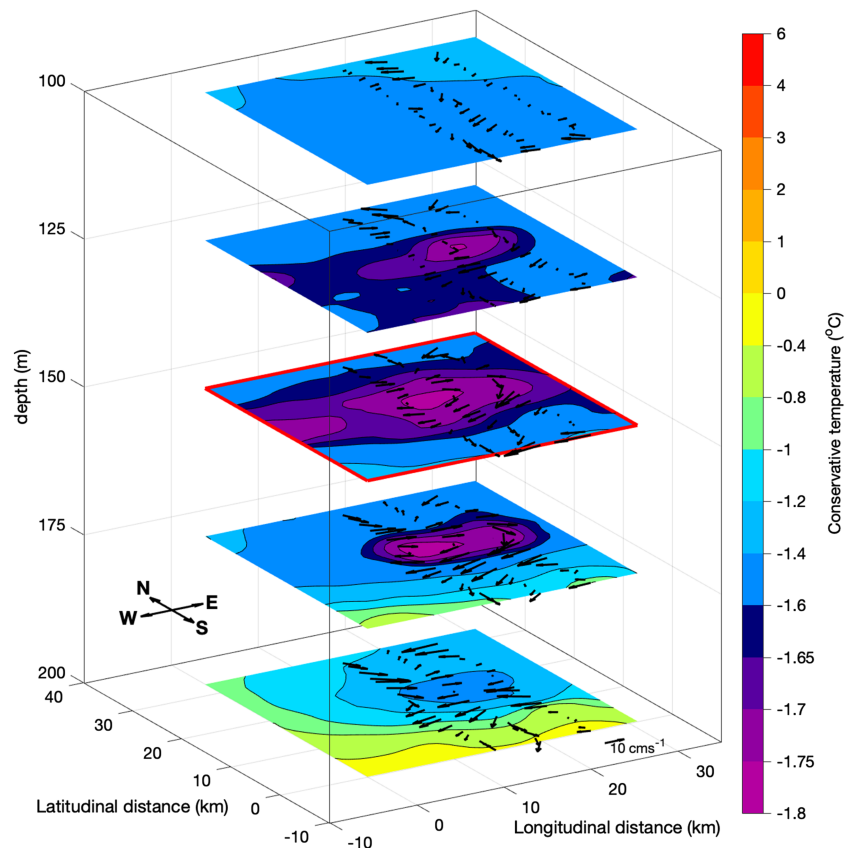

Figure 12. Lateral sections through the eddy at different depths showing the temperature (color) and velocity vectors after the slope current signature has been removed (see text for details).
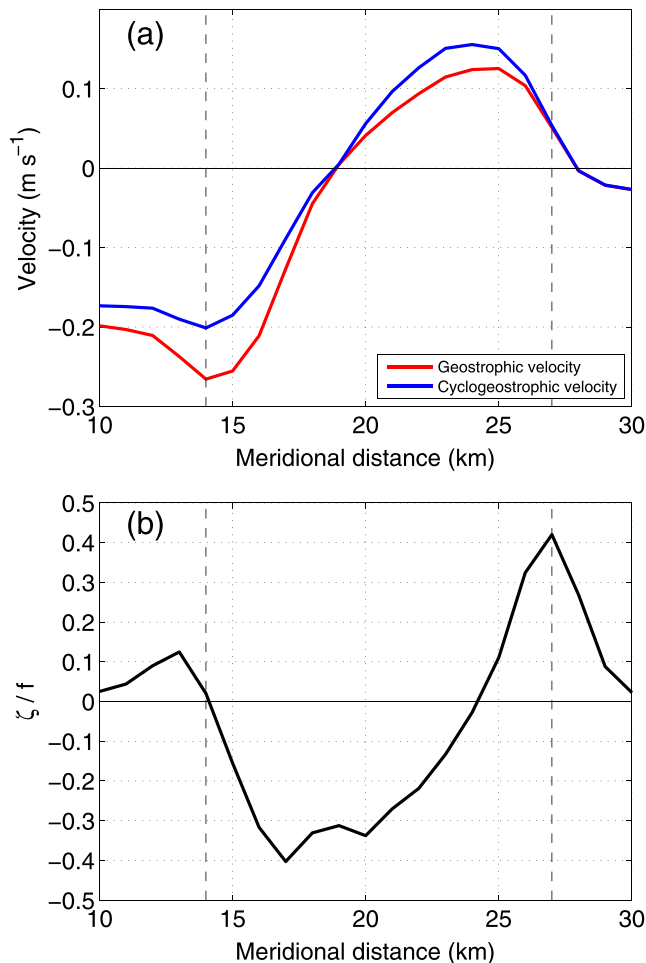
Figure 13. (a) Relative geostrophic velocity (red curve) and cyclogeostrophic velocity (blue curve) for Transect 2, averaged between the isopycnals 26.4–27.2 kg m^{-3} (see Figure 11). Both velocity terms are referenced to 250 m. (b) Rossby number along the same transect averaged within the same density layer. The vertical dashed lines are the edges of the eddy, which are visually obtained from Figure 10.

(2018), which had a similarly small Rossby number and in which the geostrophic term accounted for most of the cyclogeostrophic velocity.

4. Summary and Discussion

In this study we have presented a unique three-dimensional view of an Arctic cold-core eddy located roughly 50-km seaward of the Chukchi Sea shelfbreak over the 1,000-m isobath. It had a zonal diameter of ~19 km and a meridional diameter of ~14 km, with cold NVWW in its core centered at 150-m depth. Elevated levels of nutrients, fluorescence, and dissolved oxygen indicated biological activity within the eddy. However, the fluorescence was due to phaeopigments instead of healthy chlorophyll, indicating that photosynthesis was no longer active. This is to be expected since the eddy descended to a depth well below the euphotic depth after leaving the shelf. The chlorophyll to phaeopigment differential is consistent with the eddy age being on the order of months, which was previously deduced using radium dating (Kadko et al., 2008).

The shipboard velocity data indicated that the eddy was embedded in the offshore edge of the westward-flowing Chukchi slope current, which was surface-intensified with a volume transport roughly 0.8 Sv — similar to previous autumn measurements of the current. Subtracting out the slope current signal, we demonstrated that the eddy velocity field was symmetrical with a peak azimuthal speed of order 10 cm s^{-1}. Its Rossby number was small (~0.4), consistent with the fact that the measured cyclogeostrophic velocity was dominated by the geostrophic component. The swirl speed extended below the depth of the property core of the eddy, in line with previous modeling results (Spall et al., 2008).

Using the surface velocity field derived from the satellite absolute dynamic topography during the period of observation (see section 2.4), we are able to map out the path of the Chukchi slope current in relation to the location of the eddy (Figure 14). The eddy is situated precisely where the slope current is diverted to the north (see also Figure 9). As such, one might be tempted to think that anti-cyclonic eddy is altering the path of the current (causing the slope current to partially wrap around the eddy). It is more likely, however, that the slope current is bending northward in response to the local bathymetry of Hanna Canyon, which causes the isobaths to bend to the north.

Ours are not the only measurements revealing an intrahalocline eddy embedded in the seaward side of the Chukchi slope current. Kawaguchi et al. (2012) reported on a large, warm-core anti-cyclone similarly situated (the authors referred to the strong westward flow as a southern branch of the Beaufort Gyre. How do such eddies end up here? As noted in the introduction, the Chukchi shelfbreak jet is highly unstable and readily spawns anti-cyclonic eddies (Pickart et al., 2005; Spall et al., 2008). However, the relative locations of the Chukchi slope current and shelfbreak jet suggest that eddies formed by this process would end up getting entrained into the onshore side of the slope current not its offshore side; that is, as the eddies progress northward, they encounter the southern side of the slope current. It should be remembered, however, that the slope current is strongly influenced by wind. In particular, Li et al. (2019) demonstrated that the current is enhanced when the wind stress curl is positive on the Chukchi shelf. This is due to the decrease in sea surface height (SSH) on the shelf relative to the slope, which results in a stronger northward SSH gradient and hence stronger westward flow. By contrast, when the wind stress curl is negative on the Chukchi shelf, the slope current is retarded or absent due to the increase in SSH on the shelf versus the slope, which weakens or flattens the northward SSH gradient. Thus, eddies emanating from the Chukchi shelfbreak jet after a negative wind stress curl event might be able to progress offshore before the slope current re-establishes itself.
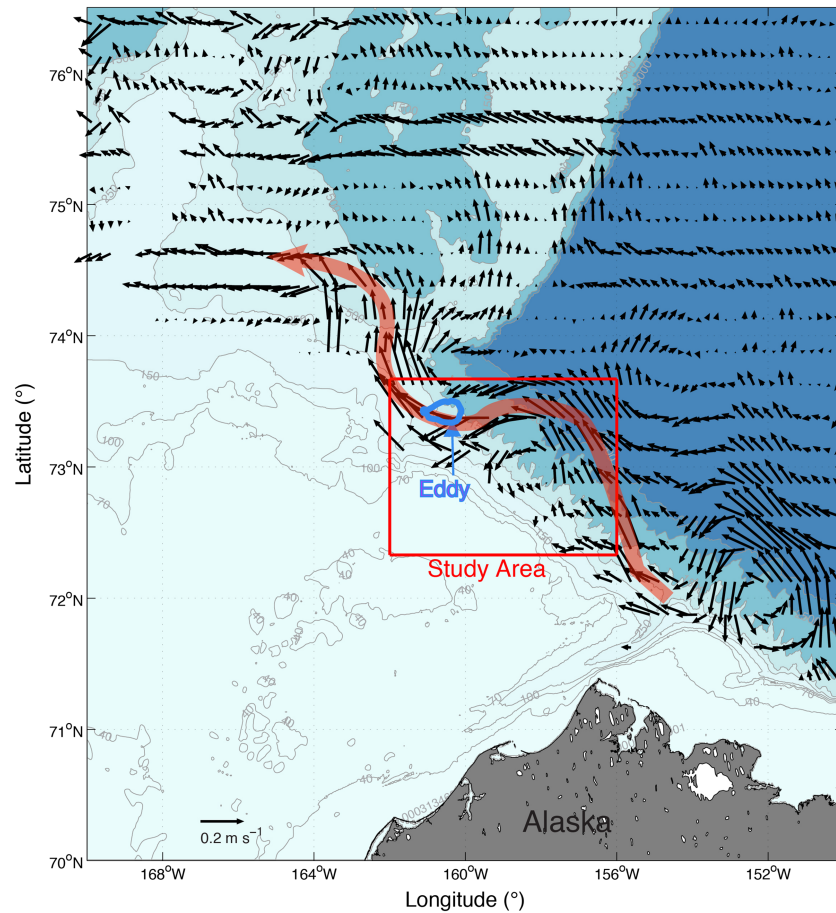
Figure 14. Surface velocity vectors derived from the absolute dynamic topography for the day of the eddy survey. The red line denotes the approximate path of the Chukchi Slope Current. The blue contour denotes the edge of the eddy (the −1.6° C contour from Figure 6). The bathymetry is from IBCAO v3 (Jakobsson et al., 2012). The study area outlined in red is shown in Figure 3.

To investigate this, we computed the time series of wind stress curl over the same region of the Chukchi shelf considered by Li et al. (2019; see Figure 2 for the region) for the time period of June to August 2004 — the hypothesis being that the eddy was formed some months before it was measured. Figure 15 shows that there were plenty of periods over this 3-month time span when the slope current might have been disrupted, allowing the eddy to move well offshore. As discussed by Spall et al. (2008), the shelfbreak eddies are originally formed as dipole pairs that self-propagate seaward. Fairly soon after formation the cyclone partner spins down, which is why there is a preponderance of anti-cyclones in the basin.
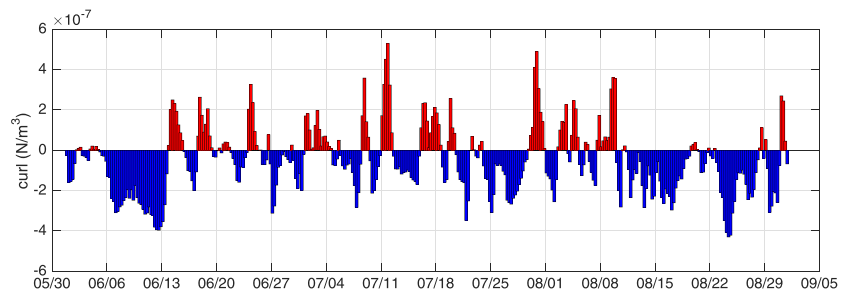

Figure 15. Time series of wind stress curl (every 6 hr) averaged over the region marked in Figure 2 on the northeast Chukchi shelf for the period June–August 2004.

It is perhaps more likely that the eddies embedded on the seaward side of the Chukchi slope current emanated from Barrow Canyon. As discussed in the Introduction, different mechanisms are believed to result in eddy formation from the canyon outflow, and eddies have been observed seaward of the canyon mouth. Hence, as the slope current forms from westward-turning flow leaving the canyon, it could influence a previously formed eddy residing farther offshore. Based on our slope current velocity data (5–10 cm s^{-1} at the offshore edge of the current, Figure 10), in this scenario the eddy would have been advected to our measurement site within 1–2 months, consistent with the estimated age of the eddy.

If this was a regular occurrence, it would mean that some fraction of the turbulent outflow from Barrow Canyon is also transported to the west, in addition to the Pacific water directly forming the slope current. Furthermore, any eddies stemming from the Chukchi shelfbreak jet under positive (or weak) wind stress curl conditions would likely follow a similar pathway via the inshore side of the slope current. One implication is that the primary geographical region of halocline ventilation in the Canada Basin — via cold-core eddies plus the Chukchi slope current — is to the west of Barrow Canyon. However, it is unknown how many eddies emanating from the canyon are entrained by the slope current, and, as noted in the Introduction, cold-core eddies are also spawned to the east by the Beaufort shelfbreak jet — although the transport of the Beaufort shelfbreak jet is roughly five times smaller than that of the Chukchi slope current. Further investigation is necessary to elucidate precisely where the halocline ventilation occurs as well as the degree to which the ventilation is accomplished via mesoscale eddies versus the advective source of the Chukchi slope current. Assessing this will be challenging in part because we do not know how often eddies are formed during the winter months.

Previous papers have addressed the spin-down of eddies in the Canada Basin. Ou and Gordon (1986) considered the effect of pack ice in retarding the eddy flow due to ocean-ice stress and estimated a decay timescale of 1–10 years. Using this methodology, Zhao et al. (2014) estimated the lifetime of their observed small, cold-core anti-cyclones to be from 0.9 to 5 years. In our case we note that the velocity signature of the eddy is absent at a depth of 150 m (Figure 12) as well as shallower than this (not shown), so it is unlikely that ice friction will impact its ultimate decay. Padman et al. (1990) considered the effect of background dissipation on the spin-down of a small cyclone located in the cold halocline layer and deduced a decay timescale on the order of 10 years. We are unable to assess the impact of small-scale mixing using our data but have no reason to suspect that the conclusion would be different than that reached by Padman et al. (1990).

Another mechanism for spinning down a cold-core anti-cyclone is due to convergence/divergence of the radial flow which can lead to vertical and horizontal exchanges of water masses. This in turn would flatten the displaced isopycnals of the eddy. Zhao et al. (2014) assessed this process for a representative eddy in their data set and deduced a much shorter decay time of roughly 7 months. Following the same methodology for the radial velocities along Transect 2 through the center of our eddy, we come up with a spin-down time on the order of half a year, which is comparable to Zhao et al.'s (2014) result. As noted above, there is NVWW outside of the eddy (i.e. the patch of cold water to the west of the eddy in the lateral map of Figure 6), which could be a reflection of this process.

A final thing to consider is, does the interaction of an eddy with the Chukchi slope current impact the eddy's decay process and spin-down time? For the cold-core eddy observed here, the onshore side of the feature was in contact with the slope current, while the offshore side of the eddy was not (or was less impacted). This would suggest that the eddy will become sheared at some point; recall that the zonal diameter of the eddy we measured was longer than its meridional diameter. This in turn implies that it would spin-down more quickly as the lateral gradients are enhanced. Further work is necessary to address this and other ramifications of eddy-slope current interactions.

References

Aagaard, K., Coachman, L., & Carmack, E. (1981). On the halocline of the Arctic Ocean. Deep Sea Research Part A. *Oceanographic Research Papers*, *28*(6), 529–545. https://doi.org/10.1016/0198-0149(81)90115-1

Anderson, L. G., Andersson, P. S., Björk, G., Jones, E. P., Jutterström, S., & Wåhlström, I. (2013). Source and formation of the upper halocline of the Arctic Ocean. *Journal of Geophysical Research: Oceans*, *118*, 410–421. https://doi.org/10.1029/2012JC008291

Arrigo, K. R., Mills, M. M., van Dijken, G. L., Lowry, K. E., Pickart, R. S., & Schlitzer, R. (2017). Late spring nitrate distributions beneath the ice-covered Northeastern Chukchi Shelf. *Journal of Geophysical Research: Biogeosciences*, *122*, 2409–2417. https://doi.org/10.1002/2017JG003881

Berrisford, P., Dee, D., Fielding, K., Fuentes, M., Kallberg, P., Kobayashi, S., & Uppala, S. (2009). The ERA-interim archive. ERA report series. (Vol. 1). (Technical Report, pp. 16). European Centre for Medium-Range Weather Forecasts, Shinfield Park, Reading.

Brugler, E. T., Pickart, R. S., Moore, G., Roberts, S., Weingartner, T. J., & Statscewich, H. (2014). Seasonal to interannual variability of the Pacific water boundary current in the Beaufort Sea. *Progress in Oceanography*, *127*, 1–20. https://doi.org/10.1016/j.pocean.2014.05.002

Carmack, E., Polyakov, I., Padman, L., Fer, I., Hunke, E., Hutchings, J., et al. (2015). Toward Quantifying the increasing role of oceanic heat in sea ice loss in the New Arctic. *Bulletin of the American Meteorological Society*, *96*(12), 2079–2105. https://doi.org/10.1175/BAMS-D-13-00177.1

Cenedese, C., & Whitehead, J. (2000). Eddy shedding from a boundary current around a cape over a sloping bottom. *Journal of Physical Oceanography*, *30*(7), 1514–1531. https://doi.org/10.1175/1520-0485(2000)030<1514:ESFABC>2.0.CO;2

Chao, S. Y., & Shaw, P. T. (2003). A numerical study of dense water outflows and halocline anticyclones in an Arctic baroclinic slope current. *Journal of Geophysical Research*, *108*(C7), 3226. https://doi.org/10.1029/2002JC001473

Codispoti, L. A., Flagg, C., Kelly, V., & Swift, J. H. (2005). Hydrographic conditions during the 2002 SBI process experiments. *Deep Sea Research Part II: Topical Studies in Oceanography*, *52*(24-26), 3199–3226. https://doi.org/10.1016/j.dsr2.2005.10.007

Cooper, L. W., Whitledge, T. E., Grebmeier, J. M., & Weingartner, T. (1997). The nutrient, salinity, and stable oxygen isotope composition of Bering and Chukchi Seas waters in and near the Bering Strait. *Journal of Geophysical Research*, *102*(C6), 12,563–12,573. https://doi.org/10.1029/97JC00015

Corlett, W. B., & Pickart, R. S. (2017). The Chukchi slope current. *Progress in Oceanography*, *153*, 50–65. https://doi.org/10.1016/j.pocean.2017.04.005

D'Asaro, E. A. (1988). Observations of small eddies in the Beaufort Sea. *Journal of Geophysical Research*, *93*(C6), 6669–6684. https://doi.org/10.1029/JC093iC06p06669

Dmitrenko, I. A., Kirillov, S. A., Forest, A., Gratton, Y., Volkov, D. L., Williams, W. J., et al. (2016). Shelfbreak current over the Canadian Beaufort Sea continental slope: Wind-driven events in January 2005. *Journal of Geophysical Research: Oceans*, *121*, 2447–2468. https://doi.org/10.1002/2015JC011514

Evans, C. A., O'Reilly, J. E., & Thomas, J. P. (1987). Part 1, A Handbook for the measurement of chlorophyll a in netplankton and nan-noplankton. In C. A. Evans, J. E. O'Reilly, & J. P. Thomas (Eds.), *A handbook for the measurement of chlorophyll a and primary production*, *BIOMASS Scientific Series* (Vol. 8, pp. 3–46). College Station, TX: Texas A & M University.

Fine, E. C., MacKinnon, J. A., Alford, M. H., & Mickett, J. B. (2018). Microstructure observations of turbulent heat fluxes in a warm-core Canada Basin Eddy. *Journal of Physical Oceanography*, *48*(10), 2397–2418. https://doi.org/10.1175/JPO-D-18-0028.1

Foukal, N. P., Pickart, R. S., Moore, G. W. K., & Lin, P. (2019). Shelfbreak downwelling in the Alaskan Beaufort Sea. *Journal of Geophysical Research: Oceans*, *124*, 7201–7225. https://doi.org/10.1029/2019JC015520

Gong, D., & Pickart, R. S. (2016). Early summer water mass transformation in the eastern Chukchi Sea. *Deep Sea Research Part II: Topical Studies in Oceanography*, *130*, 43–55. https://doi.org/10.1016/j.dsr2.2016.04.015

Holm-Hansen, O., Lorenzen, C. J., Holmes, R. W., & Strickland, J. D. (1965). Fluorometric determination of chlorophyll. *ICES Journal of Marine Science*, *30*(1), 3–15. https://doi.org/10.1093/icesjms/30.1.3

Jakobsson, M., Mayer, L., Coakley, B., Dowdeswell, J. A., Forbes, S., Fridman, B., et al. (2012). The International Bathymetric Chart of the Arctic Ocean (IBCAO) Version 3.0. *Geophysical Research Letters*, *39*, L12609. https://doi.org/10.1029/2012GL052219

Jones, E., & Anderson, L. (1986). On the origin of the chemical properties of the Arctic Ocean halocline. *Journal of Geophysical Research*, *91*(C9), 10,759–10,767. https://doi.org/10.1029/JC091iC09p10759

Kadko, D., Pickart, R. S., & Mathis, J. (2008). Age characteristics of a shelf-break eddy in the western Arctic and implications for shelf-basin exchange. *Journal of Geophysical Research*, *113*, C02018. https://doi.org/10.1029/2007JC004429

Kawaguchi, Y., Itoh, M., & Nishino, S. (2012). Detailed survey of a large baroclinic eddy with extremely high temperatures in the Western Canada Basin. *Deep Sea Research Part I: Oceanographic Research Papers*, *66*, 90–102. https://doi.org/10.1016/j.dsr.2012.04.006

Li, M., Pickart, R. S., Spall, M. A., Weingartner, T. J., Lin, P., Moore, G., & Qi, Y. (2019). Circulation of the Chukchi Sea shelfbreak and slope from moored timeseries. *Progress in Oceanography*, *172*, 14–33. https://doi.org/10.1016/j.pocean.2019.01.002

Lin, P., Pickart, R. S., Stafford, K. M., Moore, G., Torres, D. J., Bahr, F., & Hu, J. (2016). Seasonal variation of the Beaufort shelfbreak jet and its relationship to Arctic cetacean occurrence. *Journal of Geophysical Research: Oceans*, *121*, 8434–8454. https://doi.org/10.1002/2016JC011890

Linders, J., Pickart, R. S., Björk, G., & Moore, G. W. K. (2017). On the nature and origin of water masses in Herald Canyon, Chukchi Sea: Synoptic surveys in summer 2004, 2008, and 2009. *Progress in Oceanography*, *159*, 99–114. https://doi.org/10.1016/j.pocean.2017.09.005

Llinás, L., Pickart, R. S., Mathis, J. T., & Smith, S. L. (2009). Zooplankton inside an Arctic Ocean cold-core eddy: Probable origin and fate. *Deep Sea Research Part II: Topical Studies in Oceanography*, *56*(17), 1290–1304. https://doi.org/10.1016/j.dsr2.2008.10.020

Lowry, K. E., Pickart, R. S., Mills, M. M., Brown, Z. W., van Dijken, G. L., Bates, N. R., & Arrigo, K. R. (2015). The influence of winter water on phytoplankton blooms in the Chukchi Sea. *Deep Sea Research Part II: Topical Studies in Oceanography*, *118*, 53–72. https://doi.org/10.1016/j.dsr2.2015.06.006

Lowry, K. E., Pickart, R. S., Selz, V., Mills, M. M., Pacini, A., Lewis, K. M., et al. (2018). Under-ice phytoplankton blooms inhibited by spring convective mixing in refreezing leads. *Journal of Geophysical Research: Oceans*, *123*, 90–109. https://doi.org/10.1002/2016jc012575

Manley, T. O., & Hunkins, K. (1985). Mesoscale eddies of the Arctic Ocean. *Journal of Geophysical Research*, *90*(C3), 4911–4930. https://doi.org/10.1029/JC090iC03p04911

Mathis, J. T., Pickart, R. S., Hansell, D. A., Kadko, D., & Bates, N. R. (2007). Eddy transport of organic carbon and nutrients from the Chukchi Shelf: Impact on the upper halocline of the western Arctic Ocean. *Journal of Geophysical Research*, *112*, C05011. https://doi.org/10.1029/2006JC003899

Melling, H. (1993). The formation of a haline shelf front in wintertime in an ice-covered arctic sea. *Continental Shelf Research*, *13*(10), 1123–1147. https://doi.org/10.1016/0278-4343(93)90045-Y

Melling, H. (1998). Hydrographic changes in the Canada Basin of the Arctic Ocean, 1979–1996. *Journal of Geophysical Research*, *103*(C4), 7637–7645. https://doi.org/10.1029/97jc03723

Muench, R. D., Gunn, J. T., Whitledge, T. E., Schlosser, P., & Smethie, W. (2000). An Arctic Ocean cold core eddy. *Journal of Geophysical Research*, *105*(C10), 23,997–24,006. https://doi.org/10.1029/2000JC000212

Muench, R. D., Schumacher, J. D., & Salo, S. A. (1988). Winter currents and hydrographic conditions on the northern central Bering Sea shelf. *Journal of Geophysical Research*, *93*(C1), 516–526. https://doi.org/10.1029/JC093iC01p00516

Münchow, A., Falkner, K. K., & Melling, H. (2015). Baffin island and west Greenland current systems in northern Baffin bay. *Progress in Oceanography*, *132*, 305–317. https://doi.org/10.1016/j.pocean.2014.04.001

Münchow, A., Melling, H., & Falkner, K. K. (2006). An observational estimate of volume and freshwater flux leaving the Arctic Ocean through Nares Strait. *Journal of Physical Oceanography*, *36*(11), 2025–2041. https://doi.org/10.1175/JPO2962.1

Nikolopoulos, A., Pickart, R. S., Fratantoni, P. S., Shimada, K., Torres, D. J., & Jones, E. P. (2009). The western Arctic boundary current at 152 W: Structure, variability, and transport. *Deep Sea Research Part II: Topical Studies in Oceanography*, *56*(17), 1164–1181. https://doi.org/10.1016/j.dsr2.2008.10.014

Ou, H. W., & Gordon, A. L. (1986). Spin-down of baroclinic eddies under sea ice. *Journal of Geophysical Research*, *91*(C6), 7623–7630. https://doi.org/10.1029/JC091iC06p07623

Padman, L., & Erofeeva, S. (2004). A barotropic inverse tidal model for the Arctic Ocean. *Geophysical Research Letters*, *31*, L02303. https://doi.org/10.1029/2003GL019003

Padman, L., Levine, M., Dillon, T., Morison, J., & Pinkel, R. (1990). Hydrography and microstructure of an Arctic cyclonic eddy. *Journal of Geophysical Research*, *95*(C6), 9411–9420. https://doi.org/10.1029/JC095iC06p09411

Pickart, R. S. (2004). Shelfbreak circulation in the Alaskan Beaufort Sea: Mean structure and variability. *Journal of Geophysical Research*, *109*, C04024. https://doi.org/10.1029/2003jc001912

Pickart, R. S., Moore, G. W. K., Mao, C., Bahr, F., Nobre, C., & Weingartner, T. J. (2016). Circulation of winter water on the Chukchi shelf in early Summer. *Deep Sea Research Part II: Topical Studies in Oceanography*, *130*, 56–75. https://doi.org/10.1016/j.dsr2.2016.05.001

Pickart, R. S., Moore, G. W. K., Torres, D. J., Fratantoni, P. S., Goldsmith, R. A., & Yang, J. (2009). Upwelling on the continental slope of the Alaskan Beaufort Sea: Storms, ice, and oceanographic response. *Journal of Geophysical Research*, *114*, C00A13. https://doi.org/10.1029/2008jc005009

Pickart, R. S., Nobre, C., Lin, P., Arrigo, K. R., Ashjian, C. J., Berchok, C., et al. (2019). Seasonal to mesoscale variability of water masses and atmospheric conditions in Barrow Canyon, Chukchi Sea. *Deep Sea Research Part II: Topical Studies in Oceanography*, *162*, 32–49. https://doi.org/10.1016/j.dsr2.2019.02.003

Pickart, R. S., Pratt, L. J., Torres, D. J., Whitledge, T. E., Proshutinsky, A. Y., Aagaard, K., et al. (2010). Evolution and dynamics of the flow through Herald Canyon in the western Chukchi Sea. *Deep Sea Research Part II: Topical Studies in Oceanography*, *57*(1-2), 5–26. https://doi.org/10.1016/j.dsr2.2009.08.002

Pickart, R. S., Schulze, L. M., Moore, G. W. K., Charette, M. A., Arrigo, K. R., van Dijken, G., & Danielson, S. L. (2013). Long-term trends of upwelling and impacts on primary productivity in the Alaskan Beaufort Sea. *Deep Sea Research Part I: Oceanographic Research Papers*, *79*, 106–121. https://doi.org/10.1016/j.dsr.2013.05.003

Pickart, R. S., Spall, M. A., Moore, G. W. K., Weingartner, T. J., Woodgate, R. A., Aagaard, K., & Shimada, K. (2011). Upwelling in the Alaskan Beaufort Sea: Atmospheric forcing and local versus non-local response. *Progress in Oceanography*, *88*(1-4), 78–100. https://doi.org/10.1016/j.pocean.2010.11.005

Pickart, R. S., & Stossmeister, G. (2008). Outflow of Pacific water from the Chukchi Sea to the Arctic Ocean. *Chinese Journal of Polar Oceanography*, *19*(2), 135–148.

Pickart, R. S., Weingartner, T. J., Pratt, L. J., Zimmermann, S., & Torres, D. J. (2005). Flow of winter-transformed Pacific water into the Western Arctic. *Deep Sea Research Part II: Topical Studies in Oceanography*, *52*(24), 3175–3198. https://doi.org/10.1016/j.dsr2.2005.10.009

Pisareva, M. N., Pickart, R. S., Spall, M. A., Nobre, C., Torres, D. J., Moore, G. W. K., & Whitledge, T. E. (2015). Flow of pacific water in the western Chukchi Sea: Results from the 2009 RUSALCA expedition. *Deep Sea Research Part I: Oceanographic Research Papers*, *105*, 53–73. https://doi.org/10.1016/j.dsr.2015.08.011

Plueddemann, A., Krishfield, R., & Edwards, C. (1999). Eddies in the beaufort gyre. Paper presented at the Ocean-Atmosphere-Ice Interactions (OAII) All Hands Meeting, Virginia Beach, VA.

Schulze, L. M., & Pickart, R. S. (2012). Seasonal variation of upwelling in the Alaskan Beaufort Sea: Impact of sea ice cover. *Journal of Geophysical Research*, *117*, C06022. https://doi.org/10.1029/2012JC007985

Shroyer, E. L., & Pickart, R. S. (2019). Pathways, timing, and evolution of Pacific winter water through Barrow Canyon. *Deep Sea Research Part II: Topical Studies in Oceanography*, *162*, 50–62. https://doi.org/10.1016/j.dsr2.2018.05.004

Spall, M. A., Pickart, R. S., Fratantoni, P. S., & Plueddemann, A. J. (2008). Western Arctic shelfbreak eddies: Formation and transport. *Journal of Physical Oceanography*, *38*(8), 1644–1668.

Spall, M. A., Pickart, R. S., Li, M., Itoh, M., Lin, P., Kikuchi, T., & Qi, Y. (2018). Transport of Pacific water into the Canada Basin and the formation of the Chukchi Slope Current. *Journal of Geophysical Research: Oceans*, *123*, 7453–7471. https://doi.org/10.1029/2018JC013825

Steele, M., Morison, J., Ermold, W., Rigor, I., Ortmeyer, M., & Shimada, K. (2004). Circulation of summer Pacific halocline water in the Arctic Ocean. *Journal of Geophysical Research*, *109*, C02027. https://doi.org/10.1029/2003JC002009

Timmermans, M. L., Toole, J., Krishfield, R., & Winsor, P. (2008). Ice-Tethered Profiler observations of the double-diffusive staircase in the Canada Basin thermocline. *Journal of Geophysical Research*, *113*, C00A02. https://doi.org/10.1029/2008JC004829

Weingartner, T., Fang, Y. C., Winsor, P., Dobbins, E., Potter, R., Statscewich, H., et al. (2017). The summer hydrographic structure of the Hanna Shoal region on the northeastern Chukchi Sea shelf: 2011–2013. *Deep Sea Research Part II: Topical Studies in Oceanography*, *144*, 6–20. https://doi.org/10.1016/j.dsr2.2017.08.006

Weingartner, T. J., Cavalieri, D. J., Aagaard, K., & Sasaki, Y. (1998). Circulation, dense water formation, and outflow on the northeast Chukchi shelf. *Journal of Geophysical Research*, *103*(C4), 7647–7661. https://doi.org/10.1029/98JC00374

Zhao, M., & Timmermans, M. L. (2015). Vertical scales and dynamics of eddies in the Arctic Ocean's Canada Basin. *Journal of Geophysical Research: Oceans*, *120*, 8195–8209. https://doi.org/10.1002/2015JC011251

Zhao, M., Timmermans, M. L., Cole, S., Krishfield, R., Proshutinsky, A., & Toole, J. (2014). Characterizing the eddy field in the Arctic Ocean halocline. *Journal of Geophysical Research: Oceans*, *119*, 8800–8817. https://doi.org/10.1002/2014JC010488

Zhao, M., Timmermans, M. L., Cole, S., Krishfield, R., & Toole, J. (2016). Evolution of the eddy field in the Arctic Ocean's Canada Basin, 2005–2015. *Geophysical Research Letters*, *43*, 8106–8114. https://doi.org/10.1002/2016GL069671